Chinese Chemical Letters 36 (2025) 110138

Contents lists available at ScienceDirect

Chinese Chemical Letters

journal homepage: www.elsevier.com/locate/cclet

Current advances in UV-based advanced oxidation processes for the abatement of fluoroquinolone antibiotics in wastewater

Huijuan Li[a], Zhu Wang[a], Jiagen Geng[a], Ruiping Song[a], Xiaoyin Liu[b], Chaochen Fu[b], Si Li[a,*]

[a] Beijing Key Laboratory of Farmland Soil Pollution Prevention and Remediation, College of Resources and Environmental Sciences, China Agricultural University, Beijing 100193, China
[b] Beijing Water Authority, Beijing 101117, China

ARTICLE INFO

Article history:
Received 31 January 2024
Revised 23 May 2024
Accepted 17 June 2024
Available online 18 June 2024

Keywords:
UV-based advanced oxidation processes
Fluoroquinolones
Antibiotic degradation
Degradation kinetics
Transformation products

ABSTRACT

The widespread occurrence of antibiotics in wastewater aroused serious attention. UV-based advanced oxidation processes (UV-AOPs) are powerful technologies in removing antibiotics in wastewater, which include UV/catalyst, UV/H_2O_2, UV/Fenton, UV/persulfate, UV/chlorine, UV/ozone, and UV/peracetic acid. In this review, we collated recent advances in application of UV-AOPs for the abatement of fluoroquinolones (FQs) as widely used class of antibiotics. Representative FQs of ciprofloxacin, norfloxacin, ofloxacin, and enrofloxacin were most extensively studied in the state-of-art studies. The evolvement of gas-state and solid-state UV light sources was presented and batch and continuous flow UV reactors were compared towards practical applications in UV-AOPs. Generally, degradation of FQs followed the pseudo-first order kinetics in UV-AOPs and strongly affected by the operating factors and components of water matrix. Participation of reactive species and transformation mechanisms of FQs were compared among different UV-AOPs. Challenges and future prospects were pointed out for providing insights into the practical application of UV-AOPs for antibiotic remediation in wastewater.

1. Introduction

Fluoroquinolones (FQs) are broad-spectrum antibiotics that have been widely used to treat urogenital, respiratory, and gastrointestinal infections in humans and animals [1]. They were the second most commonly consumed antibiotics in humans between 2000 and 2015 across 76 countries [2] and the top commonly used antibiotics in global aquaculture in 2017 [3]. In China, the usage of FQs constituted 17% among all antibiotics [4], which was higher than those in the United States [4] and European countries [5]. After consumption, FQs are excreted unmetabolized (9.3%–86%) [4] and released into the environment. However, due to the inadequate removal of FQs in the conventional wastewater treatment plants (WWTPs) [6], they have been frequently detected in effluents of WWTPs [6,7] and surface water [8,9]. The ubiquitous occurrence of FQs potentially threats the living organisms in the aquatic environment. It has been proven that FQs could trigger acute and/or chronic toxicity to a variety of aquatic organisms such as cyanobacterium, duckweed, algae, daphnia, and fish, leading to subsequent ecological disturbance [10,11]. The emergence of FQs could also contribute to the rise and spread of antimicrobial resistance throughout the biosphere [1,6]. Therefore, development of efficient treatment technologies for FQs in wastewater is urgently needed.

In recent years, advanced oxidation processes (AOPs), mainly based on the generation of highly reactive species such as hydroxyl radicals (•OH), have shown outstanding efficiency in removing FQs [12,13]. Particularly, ultraviolet (UV)-based AOPs (UV-AOPs) stand out due to their ease of installation and operation in practical use [14], which utilize UV light and photocatalysts or chemical oxidants to decompose pollutants. Energetic UV photon could contribute higher molar absorption coefficients and quantum yields of reactive species targeting contaminants, thereby offering a potential to alleviate the overall energy consumption and reagent input. UV-AOPs have been widely implemented in practical applications [15]. Typical UV-AOPs include UV/catalyst, UV hydrogen peroxide (UV/H_2O_2), UV Fenton (UV/H_2O_2/Fe^{2+}), UV/persulfate (UV/PS), UV/chlorine, UV/ozone (UV/O_3), and UV/peracetic acid (UV/PAA) processes. UV-AOPs have been extensively tested at laboratory- or bench-scale [14] and successfully applied in removing antibiotics and other micropollutants in full-scale WWTPs [16-18]. Some review papers focused on or touched upon degradation of FQs by specific UV-AOPs such as photocatalytic oxidation [19,20], photo-

* Corresponding author.
E-mail address: sili@cau.edu.cn (S. Li).

https://doi.org/10.1016/j.cclet.2024.110138
1001-8417/

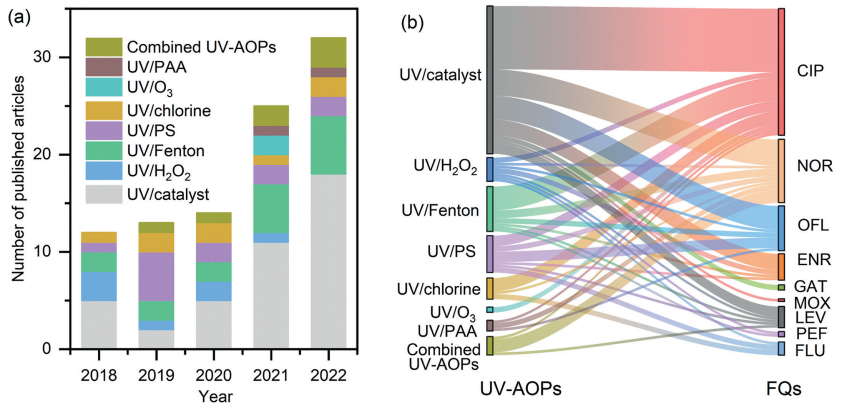

Fig. 1. Annual peer-reviewed publications on FQs degradation by UV-AOPs over the past five years (a) and distribution of UV-AOPs tested for different FQs (b).

Fenton [21,22], UV/PS [23], and UV/chlor(am)ine [24]. However, a comprehensive understanding on the fate and transformation mechanisms of FQs in different UV-AOPs is lacking.

This review aimed to summarize the current advances in application of UV-AOPs for the remediation of FQs in water in the last five years. The evolutionary trajectory of UV sources and UV reactors were summarized to shed light on the choice of light sources and reactors. The degradation kinetics of FQs and the impact of operating conditions were evaluated to provide an integrated profile of removal efficiencies of different UV-AOPs for FQs removal. The degradation mechanisms and the formation of transformation products (TPs) were compared for in-depth comprehension of reactive species participated in diverse UV-AOPs and the reactive sites of FQs. The research trends and future research directions were pointed out for providing insights into the practical application of UV-AOPs.

2. Research scope

Studies on application of UV-AOPs in removing FQs in water over the past five years (2018−2022) were retrieved by searching Web of Science (https://www.webofscience.com) with keywords of "fluoroquinolone" and "UV-AOPs/photocatalysis/UV catalyst/UV H_2O_2/UV Fenton/photo Fenton/UV H_2O_2 Fe^{2+}/UV persulfate/UV chlorine/UV ozone/UV peracetic acid". A total of 92 peer-reviewed articles were screened out covering various UV-AOPs and combined processes, and these articles increased exponentially over the past five years (Fig. 1a). Among them, UV/catalyst, as a green and sustainable process, received significant attention in removing FQs during 2018−2022. UV/PAA process has emerged attention since 2021 and the combined UV-AOPs have also been developed for efficient removal of FQs.

Fig. 1b shows the distribution of UV-AOPs tested for different FQs. The removal of nine individual FQs were investigated by UV-AOPs, including ciprofloxacin (CIP), norfloxacin (NOR), ofloxacin (OFL), enrofloxacin (ENR), levofloxacin (LEV), flumequine (FLU), gatifloxacin (GAT), moxifloxacin (MOX), and pefloxacin (PEF). The chemical structure and physiochemical properties of the nine FQs are provided in Table S1 (Supporting information). As seen from Fig. 1b, the third-generation FQs including CIP, NOR, OFL, ENR, and LEV aroused higher attention than the fourth-generation FQs such as MOX and GAT due to their higher frequency of usage. Among them, CIP was the most investigated FQ since it is commonly used in treating urinary tract infections and pneumonia, which has been frequently detected in wastewater influents and effluents [7] and global rivers [9].

3. UV sources and UV reactors

3.1. The development of UV sources and their application in UV-AOPs

The evolvement of UV light sources boosted the development of the UV-AOPs. The commonly applied UV light sources in UV-AOPs include mercury lamps, xenon pulse lamps, and UV light emitting diodes (UV-LEDs) (Fig. 2a). Conventional mercury and xenon lamps belong to the category of gas-state UV generation, while UV-LEDs are solid-state UV tubes with diverse wavelengths tuning by the solid composition of chips [25].

Conventional mercury lamps have been widely used as light source in UV-AOPs. Based on the mercury vapor pressure inside the lamp, mercury lamps are divided into high-pressure mercury (HP-Hg), medium-pressure mercury (MP-Hg), and low-pressure mercury (LP-Hg) lamps [26,27]. HP-Hg lamps produce intensified characteristic spectral lines (with maximum output at 365 nm, Fig. 2b) at high pressures (∼100 bar), with typical spectral power ranging from 50 W to 1600 W [27]. HP-Hg lamps were used in degradation of FQs in UV/H_2O_2 [28], UV/Fenton [28], and UV/PS [29,30] processes. MP-Hg lamps could emit polychromatic light (200−400 nm, Fig. 2b) at pressures of 1−10 bar [27], which were applied in UV/PAA [31] process. LP-Hg lamps were the most widely used light source in degradation of FQs in UV-AOPs, which could emit monochromatic light at 254 nm wavelength (Fig. 2b) at very low pressures (∼10^{-3} bar). Application of LP-Hg lamps for FQs removal was reported in UV/H_2O_2 [32], UV/PS [33-36], UV/chlorine [32,34,37-39], UV/O_3 [40,41], and UV/PAA [42] processes.

The xenon pulse lamp was patented in 1931 (Fig. 2a), and it is a suitable choice to simulate sunlight in UV-AOPs due to its high luminance, small size, and similar energy distribution to that of natural sunlight. Xenon lamps were used in degradation of FQs in UV/catalyst [43-52] and photo-Fenton [53,54] processes. However, the conventional gas-state UV light sources especially mercury lamps are reported to have insufficient luminous efficiency, high energy consumption, high operating temperature, short life span, and health risks of exposure to mercury [55,56]. Meanwhile, the production, import, and export of mercury-containing lamps have been completely banned by the Minamata Convention on Mercury since 2020.

The energy efficient and environment friendly UV-LEDs have become a promising alternative in UV-AOPs. UV-LEDs can emit flexible pulsed irradiation to suit specific requirements such as 275 nm [57], 365 nm [56,58], and 385 nm [59]. After decades of development, the wall-plug efficiency (WPE) of UV-LEDs has improved ∼10 times (from less than 1% to 10.1%) and their output power has jumped from <10 mW to 1.88 W. Currently, the lifetime of UV-LEDs could reach 20,000 h and the cost could be less

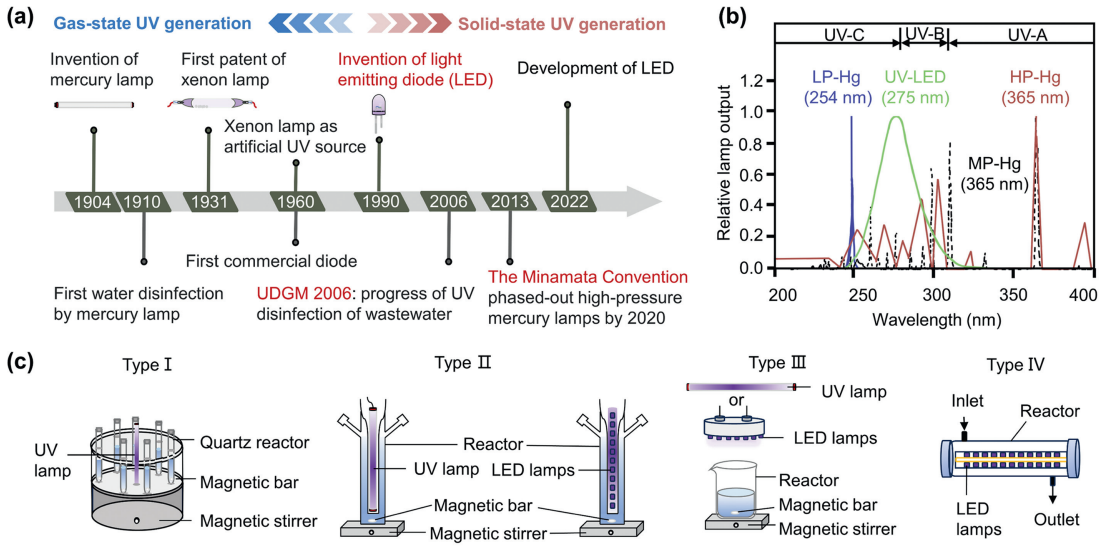

Fig. 2. The development of UV light sources (a) and their emission spectrums (b). Typical UV-AOP reactors (c).

than 0.1 USD/mW [25]. UV-LEDs has emerged great potential in the elimination of FQs by UV/catalyst [56,58,60], UV/H_2O_2 [57], UV/PS [59], and UV/chlorine [57] processes.

3.2. UV reactor configuration

The schematic illustration of the main UV-AOP reactors is presented in Fig. 2c. Generally, four types of experimental apparatus were constructed depending on the configuration of lamps and reactors. The first three types (Type I–III) are batch reactors while the Type IV reactor is a continuous flow reactor. The merry-go-round reactor, as the first type UV-AOP reactor (Type I, Fig. 2c), has been widely used in UV/catalyst [52,61], UV/H_2O_2 [28,62], UV/Fenton [28], UV/PS [30,62], and UV/PAA [42] processes. Typically, a merry-go-round reactor is an apparatus in which several quartz tubes are rotated around a mercury/xenon lamp to be exposed to equal amounts of radiation (Type I, Fig. 2c). It allows multiple sets of reactions to be performed at the same time. The Type II reactor (Fig. 2c) is equipped with a gas-state UV lamp or several LED lamps with a quartz sleeve, which is housed in the center of a cylindrical container axially along the length of the container. The application of Type II reactor was reported in UV/H_2O_2 [32], UV/chlorine [32,38,57,63], and UV/O_3 [40] processes. The Type III reactor (Fig. 2c) is comprised of a mercury lamp or LED lamps placed above a stirred tank, which was reported in UV/catalyst [56,58], UV/chlorine [37,39] processes. Different from these batch reactors, a continuous flow reactor (Type IV, Fig. 2c) is equipped with a cylindrical reactor exposed to UV irradiation of LED lamps, which are evenly distributed in the inner wall of the reactor. The compact LED lamps offer design flexibility of the UV-AOP reactors, which can potentially be used in practical applications.

4. Assessment of the degradation kinetics of FQs in UV-AOPs

The formation of the main reactive species in different UV-AOPs is illustrated in Fig. 3a, with the standard electrode potential (E0) values shown in Fig. 3b [64-67].

4.1. UV/catalyst

UV photocatalytic oxidation is the most widely reported UV-AOPs in the decomposition of FQs in wastewater owing to its environmental friendliness and satisfactory efficiency. In the photocatalysis process, organic pollutants can be degraded and even mineralized into non-toxic low molecules such as CO_2 and H_2O. Semiconductors have been widely used as photocatalysts, which are chemically stable, inexpensive, and long-lived [20].

Semiconductors can be initiated by light with energy equal or superior to the band-gap between its valence band (VB) and conduction band (CB) (Fig. 3a). After irradiation, electrons (e^-) in the VB are transferred to the CB, leaving the photogenerated hole (h^+) in the VB (Eq. 1). Then, e^- could react with oxygen (O_2) adsorbed on the semiconductor to generate superoxide radicals ($^{\bullet}O_2^-$) (Eq. 2). Further, $^{\bullet}O_2^-$ could react with H^+ and generate hydroperoxyl radicals ($^{\bullet}HO_2$) (Eq. 3). Meanwhile, h^+ could react with the surface adsorbed H_2O to form $^{\bullet}OH$ (Eq. 4), which is the predominant reactive species in photocatalysis. The oxidants of $^{\bullet}OH$ and h^+ could react with organic contaminants (Eqs. 5 and 6), leading to the degradation of parent compounds and the formation of TPs. The electron-hole recombination could occur in nanoseconds with dissipation of heat (Eq. 7).

$$\text{Semiconductor} + h\nu \rightarrow h^+ + e^- \quad (1)$$

$$e^- + O_2 \rightarrow {}^{\bullet}O_2^- \quad (2)$$

$${}^{\bullet}O_2^- + H^+ \rightarrow {}^{\bullet}HO_2 \quad (3)$$

$$h^+ + H_2O \rightarrow {}^{\bullet}OH + H^+ \quad (4)$$

$${}^{\bullet}OH + \text{organics} \rightarrow \text{TPs} \quad (5)$$

$$h^+ + \text{organics} \rightarrow \text{TPs} \quad (6)$$

$$h^+ + e^- \rightarrow \text{heat} \quad (7)$$

Table S2 (Supporting information) provides an overview of recent work on photocatalytic degradation of FQs. Seven FQs including CIP, ENR, NOR, OFL, LEV, GAT, and MOX were reported by using a large variety of inorganic and organic photocatalysts. These catalysts can be classified into metal-based, carbon-based,

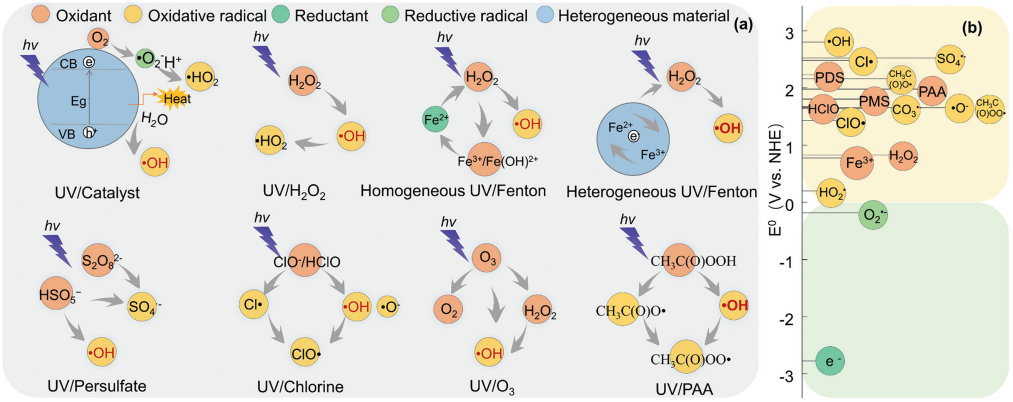

Fig. 3. Schematic illustration of the formation of reactive species in different UV-AOPs (a) and standard electrode potential (E^0) of the involved reagents and reactive species (b, data obtained from [64-67]).

and metal–carbon hybrid catalysts. Among the metal-based catalysts, metal oxides (*e.g.*, titanium dioxide (TiO_2) [56,58,68], zinc oxide (ZnO) [69]), and metal sulfides (*e.g.*, cadmium sulfide (CdS [70]) were widely used in degrading FQs under UV light irradiation. TiO_2 was the most widely used due to its outstanding activity, photochemical stability, low-cost, and relatively low toxicity [20,71]. However, owing to the wide band gap of TiO_2 (3.20 eV) [58,72], it can only be activated by UV light with wavelength shorter than 384 nm (approximately 4% of the solar light spectrum), which limits its practical application.

To reduce the recombination of electron-hole and expand the spectral response, synthesis of metal-based heterostructures and elemental doping of metal oxides have been developed [72]. For example, metal-based composites such as CdS/TiO_2 [72], ZnO/CdS [73], and CeO_2/ZnO [74] were used in FQs degradation to enhance their photocatalytic activity under visible or UV light. At the same time, elemental doping of metal oxides by transition metals (*e.g.*, Fe [75], Ag [75], and Au [48]), and non-metal elements (*e.g.*, N [68]) were reported in previous studies. Recently, the bismuth (Bi)-based catalysts have aroused extensive attention as a visible-light responsive photocatalyst, given its narrow band gap (mostly less than 3.0 eV), photostability, efficiency, and low cost [76]. For example, BiOCl [77] and ZnO/Bi_2WO_6 heterojunctions [78] were applied in degradation of NOR, CIP, and OFL under UV and visible light irradiation.

Carbon-based catalysts especially graphitic carbon nitride (g-C_3N_4) are widely used in photocatalytic degradation of pollutants, due to the advantage of metal-free, low cost, and the ability to absorb visible light with the bandgap energy of ~2.7 eV [79]. It was reported that ENR, LEV, and NOR could be fully removed under visible light in less than 60 min, when using oxygen- and nitrogen-linked g-C_3N_4 organic polymer (OCN) [51] and inverse opal potassium-doped g-C_3N_4 (K-g-C_3N_4) [47] as catalysts.

Recently, metal-carbon hybrid catalysts offer highly competitive options in degrading FQs with synergistic advantages from metal oxides and porous carbon. On one hand, carbon materials are commonly used as supports for metal oxides, which significantly increase the active surface area of the catalysts. For example, a variety of metal–carbon hybrid catalysts, such as sepiolite and zeolite TiO_2 composites [68], graphitized mesoporous carbon (GMC)/TiO_2 [80], TiO_2/powered active carbon composites (TiO_2/PAC) [81], reduced graphene oxide (rGO)/In_2TiO_5 [50], and TiO_2 coated alkali-cooking modified rice straw fiber (TiO_2@AMSF) [82] have been reported to show efficient removal of FQs under UV and visible light irradiation. On the other hand, metal oxides have been used to enhance the photocatalytic activities of carbon-based materials such as g-C_3N_4, 2D/2D N-ZnO/g-C_3N_4 S-scheme heterojunction [83], shuttle-like CeO_2/g-C_3N_4 composite [79], and $LaFeO_3$/g-C_3N_4/$BiFeO_3$ (LCB) double Z-scheme structure [45]. For instance, LCB exhibited an better photoactivity than g-C_3N_4 towards the degradation of CIP, with the pseudo-first-order rate constants (k) increased from 0.012 min^{-1} to 0.058 min^{-1} [45].

In addition, metal-organic frameworks (MOFs) are emerged as attractive photocatalysts with large surface area, ultrahigh porosity, and tailored structure [46,84]. For example, iron-doped copper 1,4-benzenedicarboxylate MOFs (Fe_3O_4/CuO@C) [46] and Bi_5O_7I/UiO-66-NH_2 heterojunction [44] showed visible light-driven photocatalytic activity towards CIP removal, with k values of 0.028 min^{-1} and 0.014 min^{-1}, respectively.

4.2. UV/H_2O_2 and UV/Fenton

UV/H_2O_2 process has been a popular treatment technique to degrade organic contaminants in water due to its high efficiency, sludge-free operation, and low investment cost [85]. It has been applied in potable water reuse at full scale [86]. Photolysis of H_2O_2 by UV irradiation (usually 254 nm) could break the O–O band and generate ·OH (Eq. 8 and Fig. 3a) [28,62]. UV/H_2O_2 process showed efficient removal of a variety of FQs, with the maximum removal efficiencies ranging from 86.0% to 100% (Table S3 in Supporting information).

$$H_2O_2 + h\nu \rightarrow 2{\cdot}OH \quad (8)$$

UV/Fenton is a classic Fenton-related oxidation process which relies on the synergistic action of UV and Fenton's reagent (H_2O_2/Fe(II)). In comparison with the conventional Fenton reaction, the introduction of UV light increases the efficiency of Fenton reagent in oxidizing organic compounds and conserves dosage of Fenton reagent [28]. UV/Fenton is comprised of homogenous UV/Fenton process and heterogeneous UV/Fenton process. The formation of reactive species in these two processes is illustrated in Fig. 3a.

In the homogenous UV/Fenton process, $Fe^{2+}$and H_2O_2 drive the generation of ·OH and Fe^{3+} under UV irradiation (Eq. 9) [13,87]. Fe^{3+} and OH^- in the water could be complexed to form $Fe(OH)^{2+}$, which can further be reduced to Fe^{2+} under UV irradiation with the generation of ·OH (Eq. 10) [22,84]. Thus, the accelerated cycle of Fe^{2+}/Fe^{3+} promotes the utilization efficiency of H_2O_2, leading to the enhancement of antibiotic removal [28].

$$Fe^{2+} + H_2O_2 \rightarrow Fe^{3+} + {\cdot}OH + OH^- \quad (9)$$

$$Fe(OH)^{2+} + h\nu \rightarrow Fe^{2+} + {\cdot}OH \quad (10)$$

Homogenous UV/Fenton process has been applied in removing FQs (Table S4 in Supporting information); however, it suffers from poor pH adaptability [84] and low Fe^{2+} utilization [88]. Thus, the development of heterogeneous UV/Fenton process attracted increasing attention, where Fe-containing solid catalysts were employed to initiate UV/Fenton reaction as replacement of Fenton reagents (Table S5 in Supporting information). Compared with the homogenous UV/Fenton process, $^{\bullet}OH$ could be generated on the surface of catalysts from the heterogeneous catalytic decomposition of H_2O_2 in heterogeneous UV/Fenton process (Fig. 3a), which enhances the degradation efficiency and widens the pH adaptability [21,88]. In addition, the heterogeneous catalysts could be recycled and reused to reduce the cost [88]. Different kinds of heterogeneous catalysts were synthesized and applied in photo-Fenton process for the removal of FQs under UV or visible light, including nanoscale zero valent iron (nZVI) [89], rGO-$ZnFe_2O_4$ [53], FeCu/rGO [90], highly dispersed FeC_6 on sepiolite (Fe-Dis@Sep) [54], Fe-based MOFs (L-MIL-53(Fe, Mn) and L-MIL-53(Fe, Cu) (MIL: Material of Institute Lavoisier) [84], Fe_3O_4@MIL-100(Fe) [91], and Fe-TCPP consisting of TCPP ligands and Fe-O cluster ($Fe_3O(COO)_6$) [92]).

4.3. UV/persulfate

UV/PS process exhibits great application prospect in the removal of organic pollutants, which relies on the generation of strong oxidant reactive species of $SO_4^{\bullet-}$ ($E^0 = 2.44$ V *vs.* NHE) and $^{\bullet}OH$ (E^0 =2.73 V *vs.* NHE) (Fig. 3b) [64]. $SO_4^{\bullet-}$ and $^{\bullet}OH$ could be produced through the activation of peroxymonosulfate (PMS, HSO_5^-/SO_5^{2-}) or peroxydisulfate (PDS, $S_2O_8^{2-}$) by different activation methods including UV irradiation, heat, ultrasonic irradiation, transition metals, *etc.* [65,93]. Compared with other activation methods, UV/PS is regarded as an efficient, environmentally friendly, and cost-effective approach for the elimination of pollutants under mild conditions [94]. Our statistical results also indicate significant differences of the k values among different UV-AOPs ($P < 0.001$, one-way ANOVA, Fig. S1 in Supporting information). The superiority of UV/PS compared to UV/catalyst ($P < 0.001$, Dunn's test), UV/H_2O_2 ($P < 0.01$, Dunn's test), and UV/Fenton ($P < 0.001$, Dunn's test) processes was further elucidated based on the data contained in this review.

UV/PS involves the breakage of the peroxide bond in PMS (Eq. 11) and PDS (Eq. 12) by the energy input from UV light to generate $SO_4^{\bullet-}$ and $^{\bullet}OH$ (Fig. 3a) [94]. Meanwhile, $SO_4^{\bullet-}$ could be transformed to $^{\bullet}OH$ especially under alkaline conditions (Eq. 13) [93]. In comparison with $^{\bullet}OH$, $SO_4^{\bullet-}$ has higher selectivity, higher oxidation capacity, wider range of pH, and longer half-life [93].

$$HSO_5^- + h\nu \rightarrow SO_4^{\bullet-} + {}^{\bullet}OH \quad (11)$$

$$S_2O_8^{2-} + h\nu \rightarrow 2SO_4^{\bullet-} \quad (12)$$

$$SO_4^{\bullet-} + OH^- \rightarrow SO_4^{2-} + {}^{\bullet}OH \quad (13)$$

Recent studies of UV/PS in FQs elimination are summarized in Table S6 (Supporting information). As seen, UVC-activated PS is more preferred in degradation of FQs since FQs are reported to have a significant absorption at ~275 nm UVC (π–π^* transition of aromatic ring) [58]. Degradation of FQs was widely reported in previous studies by using 254 nm UVC to activate PMS or PDS [33-35,62]. Tentatively, UV/PS degradation of NOR and OFL was conducted under vacuum UV (VUV, 185 nm) [95], and VUV/PS showed rapid removal of NOR and OFL with the removal efficiency of almost 100% within 3 min.

Milh and his co-workers compared the efficiency of UV/PDS and UV/PMS processes for the removal of CIP in wastewater. They found that UV/PDS was superior to UV/PMS, with the k values of 0.752 and 0.145 min^{-1}, respectively [33]. This is attributed to the lower O−O band dissociation energy (140 kJ/mol) in PDS than that in PMS (377 kJ/mol) [94]. Accordingly, less energy is required by PDS to produce radicals in the cleavage of peroxide bond. The performance of UV/PS process was further compared with other UV-AOPs. Compared with UV/H_2O_2 process, UV/PDS oxidation was substantially more efficient in removing OFL and LEV [62]. The k values of OFL and LEV were 1.67−1.95 and 1.36−2.05 times higher in UV/PDS than those in UV/H_2O_2 under different pH conditions (3−11). Accordingly, the total cost of OFL and LEV removal by using UV/PDS process reduced by 40.8% and 24.8%, respectively, indicating that UV/PDS process is more economically competitive than UV/H_2O_2 process.

4.4. Other UV-AOPs

Degradation of FQs by other UV-AOPs including UV/chlorine, UV/O_3, UV/PAA, and the combination of UV-AOPs was also reported, with details presented in the following section.

4.4.1. UV/chlorine

UV/chlorine, coupling chlorine with a UV light source, is an attractive alternative in the UV-AOPs for FQs removal. Chlorine (*e.g.*, Cl_2, ClO_2 or sodium hypochlorite (NaClO)) reacts with water to form hypochlorous acid (HOCl) and hypochlorite ion (ClO^-), which acts as oxidants under UV irradiation [32,34,37-39,57] to produce $^{\bullet}OH$ and reactive chlorine species (RCS) of $Cl^{\bullet}$ and $ClO^{\bullet}$ (Eqs. 14−18) (Fig. 3a) [86]. $Cl^{\bullet}$ and $ClO^{\bullet}$ are powerful oxidants with oxidation potentials of 2.43 V *vs.* NHE and 1.39 V *vs.* NHE, respectively (Fig. 3b) [64]. RCS preferentially react with electron-rich moieties and their concentrations could be several orders of magnitude higher than that of $^{\bullet}OH$ in UV/chlorine process [32].

$$HOCl/OCl^- + h\nu \rightarrow {}^{\bullet}OH/{}^{\bullet}O^- + Cl^{\bullet} \quad (14)$$

$$^{\bullet}OH + HOCl \rightarrow ClO^{\bullet} + H_2O \quad (15)$$

$$^{\bullet}OH + OCl^- \rightarrow ClO^{\bullet} + OH^- \quad (16)$$

$$Cl^{\bullet} + HOCl \rightarrow ClO^{\bullet} + H^+ + Cl^- \quad (17)$$

$$Cl^{\bullet} + OCl^- \rightarrow ClO^{\bullet} + Cl^- \quad (18)$$

Degradation of FQs by UV/chlorine was reported by using 254 nm [34,37,39,96] and 275 nm [57] UV light (Table S7 in Supporting information). For example, 98.9% of CIP could be removed in 10 min by UV/chlorine in reclaimed water from a water resource recovery facility, with a k value of 0.6214 min^{-1}, which was comparable to that in UV/PDS process [34]. At the same time, the k value of CIP degradation in UV/chlorine process was 3.2 and 3.7 times higher than that of UV/H_2O_2 and direct UV in reclaimed water [34]. The electrical energy per order (E_{EO}) followed the order of direct UV (2.23 kWh/m^3) > UV/H_2O_2 (1.91 kWh/m^3) > UV/chlorine (0.84 kWh/m^3) ≈ UV/PDS (0.76 kWh/m^3). Another study showed that compared with the UV/H_2O_2 process, UV/chlorine achieved better removal of 28 micropollutants including FLU in simulated drinking water and wastewater at the same molar oxidant dosage [32]. The UV/chlorine process was less affected by wastewater matrices than UV/H_2O_2. In addition, the UV/chlorine process saved 46.4% and 80.0% E_{EO} for FLU removal than UV/H_2O_2 process in simulated drinking water and wastewater, respectively [32]. The

superior efficiency and economical feasibility of UV/chlorine over UV/H_2O_2 in FQs elimination were also reported previously [57,96]. However, the biotoxicity of the chlorinated byproducts arising from FQs degradation in UV/chlorine process should be evaluated in view of health concerns [37,39,63]. It was reported that haloacetic acids (HAAs) and non-HAAs disinfection byproducts formed in UV/chlorine process contributed to the enhanced toxicity than UV alone [63].

4.4.2. UV/O_3

UV/O_3 process is feasible for the treatment of FQs wastewater owing to the strong oxidation capacity. O_3 strongly absorbs UV light at 254 nm and produces H_2O_2 (Eq. 19), which can be decomposed to $^{\bullet}$OH (Eq. 20) [41]. O_3 could also react with H_2O_2 to yield $^{\bullet}$OH (Eq. 21) [13,41]. The schematic illustration of the formation of reactive species in UV/O_3 process can be found in Fig. 3a.

$$O_3 + H_2O + h\nu \rightarrow H_2O_2 + O_2 \quad (19)$$

$$H_2O_2 + h\nu \rightarrow 2^{\bullet}OH \quad (20)$$

$$H_2O_2 + 2O_3 \rightarrow 2^{\bullet}OH + 3O_2 \quad (21)$$

A pilot-scale study demonstrated that CIP could be fully removed in 6 min by (V)UV/O_3 in biologically treated wastewater from two medium-sized WWTPs (Table S8 in Supporting information), with E_{EO} values of 1.1 and 1.6 kWh/m^3, respectively [41]. The UV/O_3 process was also effectively applied in treating high-salinity organic wastewater, with toxicity of TPs similar or less than that of CIP [40].

4.4.3. UV/PAA

The UV/PAA process emerged as an alternative in pollutants abatement. Commercial PAA ($CH_3C(O)OOH$) solution contains a mixture of PAA, acetic acid (CH_3COOH), H_2O_2, and H_2O (Eq. 22), with concentrations of 5%–15% (mainly 12%) [86,97]. H_2O_2 participates in the perhydrolysis process, facilitating subsequent redox reactions with the powerful oxidant PAA (E^0 =1.96 V *vs.* NHE) (Fig. 3b) [66,98].

$$CH_3COOH + H_2O_2 \rightarrow CH_3C(O)OOH + H_2O \quad (22)$$

Under UV irradiation, the O−O band in PAA is cleaved, resulting the formation of $^{\bullet}$OH and a series of organic peroxyl radicals including acetyloxyl radical ($CH_3C(O)O^{\bullet}$, E^0 =2.24 V *vs.* NHE) and acetylperoxyl radical ($CH_3C(O)OO^{\bullet}$, E^0 =1.60 V *vs.* NHE) (Eqs. 23−25) (Figs. 3a and b) [31,67,99].

$$CH_3C(O)OOH + h\nu \rightarrow CH_3C(O)O^{\bullet} + {}^{\bullet}OH \quad (23)$$

$$CH_3C(O)OOH + {}^{\bullet}OH \rightarrow CH_3C(O)OO^{\bullet} + H_2O \quad (24)$$

$$CH_3C(O)OOH + CH_3C(O)O^{\bullet} \rightarrow CH_3C(O)OO^{\bullet} + CH_3C(O)OH \quad (25)$$

The UV/PAA process was used in decontamination of CIP, LEV, NOR, and OFL in previous studies (Table S9 in Supporting information) [31,42,99]. UV/PAA significantly promoted the degradation of FQs compared to UV alone and the PAA process due to the formation of $^{\bullet}$OH and carbon-centered organic radicals. In addition, UV/PAA achieved higher removal efficiencies of CIP, NOR, and OFL than UV/NaClO process in wastewater from effluent of a municipal WWTP [42].

4.4.4. Combination of UV-AOPs

Combination of UV-AOPs was applied in FQs removal to achieve a positive synergy effect (Table S10 in Supporting information). For example, photocatalytic activation of PS was successfully applied in the removal of NOR [79,100-102] and CIP [103] in wastewater. Photocatalytic activation of PS greatly improved the degradation of FQs than heterogeneous catalysts-mediated activation of PS [79,100], UV/PS [102], and photocatalysis [102]. The photogenerated e^- could react with PS to generate $SO_4^{\bullet-}$ and $^{\bullet}$OH (Eqs. 26−28) [79,94], simultaneously inhibiting the recombination of e^-−h^+ pairs and promoting the efficiency of the charge carriers.

$$HSO_5^- + e^- \rightarrow SO_4^{\bullet-} + OH^- \quad (26)$$

$$HSO_5^- + e^- \rightarrow SO_4^{2-} + {}^{\bullet}OH \quad (27)$$

$$S_2O_8^{2-} + e^- \rightarrow SO_4^{\bullet-} + SO_4^{2-} \quad (28)$$

A previous study reported that 98% of NOR was removed in 60 min in a UV/TiO_2@nZVI/PS system [100]. Wu and his co-workers found that the degradation rate of NOR by UV/PDS increased by 45.8% with the addition of a composite of nitrogen-doped graphene (NGO) and Fe_3O_4, with the *k* value enhanced by 1.94 and 13.12 times compared to UV/PDS and UV/NGO-Fe_3O_4 processes [102]. Apart from the direct electron transfer activation of PS as stated in Eqs. 26−28, the synergistic effect was also attributed to the indirect electron transfer activated by Fenton-like catalysts [94]. Tian and his co-workers compared the removal of NOR by three co-catalytic photo-Fenton-like processes including WO_3/Fe^{2+}/PMS, $WO_3/Fe^{2+}/H_2O_2$, and WO_3/Fe^{2+}/PDS under visible light [104]. Among them, the PMS-based process showed the highest removal efficiency of NOR and the highest mineralization rate.

4.5. Effects of operation conditions on FQs degradation

The degradation kinetics of FQs in UV/AOPs is strongly affected by the UV light intensity, dosage of catalysts/oxidants, initial concentration of FQs, solution pH, and water matrix components [12,14,33,105]. UV light intensity is crucial in UV/AOPs and degradation of FQs was found to be positively affected by the UV power due to promoted direct photolysis and generation of reactive species [33,39,106]. The effect of catalyst/oxidant dosage on the *k* values of FQs in typical UV-AOPs is shown in Figs. 4a–d. As seen, the *k* values of FQs were gradually increased at higher concentrations of catalyst [44-46,51,72,77,107-110] (Fig. 4a), H_2O_2 [28,32,62,85,111] (Fig. 4b), Fe^{2+} [28,112,113] or Fe-based heterogeneous catalyst (Fig. 4c) [53,54,84,90,91,114], or persulfate (Fig. 4d) [30,34-36,62,95,115,116], because higher dosage of catalyst/oxidant enhanced the formation of reactive species such as $^{\bullet}$OH. However, excessive dosage of catalyst/oxidant resulted in radical scavenging with the formation of less reactive species and the degradation was inhibited [28,62]. In the heterogeneous UV-AOPs, overdose of catalyst decreased the catalytic efficiency by light screening and loss of active sites due to catalyst aggregation [51,91,107,114].

The effect of initial concentration of FQs on degradation kinetics was extensively investigated in UV-AOPs. The initial concentration of FQs negatively affected the *k* values of FQs in UV/catalyst [45,47,51,70,72,77,83,107,108,110,117,118], UV/Fenton [53], and UV/PS [115] processes, due to the competition for the active sites of the catalyst and the reactive species at higher concentration of FQs. In addition, the degradation kinetics was pollutant-dependent in UV-AOPs. Take photocatalysis process for example, some studies showed that OFL had faster degradation than NOR

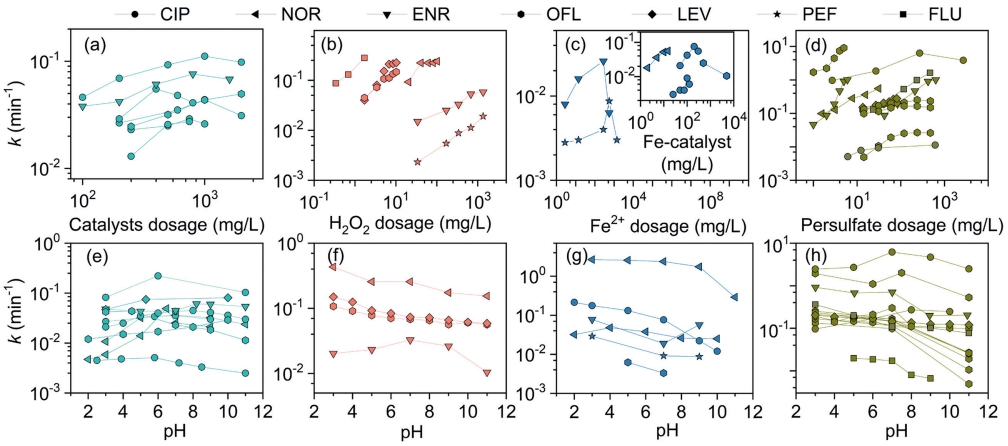

Fig. 4. Effect of catalyst/oxidant dosage and pH on the *pseudo*-first-order rate constants (k) of FQs during UV/catalyst (a, e), UV/H_2O_2 (b, f), UV-Fenton (c, g), and UV/persulfate (d, h).

and CIP [60,77,78], while LEV and ENR exhibited faster degradation than NOR and CIP [60,83]. However, another study reported that NOR had a higher degradation rate than LEV in CdS-photocatalysis under UVA light [70]. The inconsistence in the pollutant-dependent activities of FQs in UV-AOPs could be related to the discrepancy in the adsorption of FQs on the catalyst, absorption of photons, and thermodynamic and kinetic barriers resulting from structural differences among different FQs [119,120]. The impact of structural factors on the photochemical fate of FQs needs to be further clarified by experimental and theoretical evidence.

Solution pH is critical for the degradation of FQs in UV-AOPs, which strongly affected the dissociation of FQs, the surface charge of catalyst, and the concentrations and speciation of radicals [31,58]. In photocatalysis process, FQs degradation was favored in neutral or nearly neutral conditions when the zwitterionic form of FQs dominated (Fig. 4e and Fig. S2 in Supporting information) [44-46,58,72,77,78,82,83,107,108,117,118,121]. However, in strong acidic or alkaline environment, the electrostatic repulsion between ionic FQs and catalysts hindered the adsorption of FQs on the catalyst and the corresponding degradation. In UV/H_2O_2 and UV/Fenton processes, acidic condition was favorable for FQs degradation (Figs. 4f and g, and Fig. S2 in Supporting information). The optimum pH value was 3 in UV/H_2O_2 [62,85,122] and homogeneous UV/Fenton [28,104,113], since H_2O_2 could be dissociated to form hydroperoxy anions (HO_2^-) as aggressive agent of H_2O_2 and $^{\bullet}OH$ in alkaline solutions [28,62]. In addition, the decrease in the oxidation potential of $^{\bullet}OH$ with increasing pH and the formation and precipitation of iron complex at pH > 4 further inhibited FQs degradation [28,104]. In UV/PS, $SO_4^{\bullet-}$ was the main active species under acidic condition while $^{\bullet}OH$ became dominant under alkaline condition (Eq. 13). Previous studies reported that the degradation efficiency of FQs decreased with increasing pH in UV/PS (Fig. 4h) [29,30,36,62,116] due to the lower reactivity of $^{\bullet}OH$ than that of $SO_4^{\bullet-}$. However, other studies showed that neutral condition was most favorable for FQs degradation [34,95,123] (Fig. 4h and Fig. S2 in Supporting information) since the zwitterionic form of FQs had the highest reactivity towards the electrophilic attack.

Inorganic ions and dissolved organic matter (DOM) are ubiquitous in water, which could significantly influence the degradation of FQs in UV-AOPs [14,105]. Previous studies revealed that the coexisting cations (Na^+, K^+, Ca^2, Mg^{2+}, Cu^{2+}, and Fe^{3+}) [53,62,85,113,116] and anions (NO_3^-, Cl^-, Br^-, $H_2PO_4^-$, HCO_3^-, CO_3^{2-}, and SO_4^{2-}) [29,30,44,62,85,111,113,116,123] could inhibit FQs degradation in UV-AOPs by radical quenching. For example, cations inhibited the removal of NOR in UV/H_2O_2 in the order of Cu^{2+} > Ca^{2+} > Mg^{2+} due to the coordination between NOR and the divalent metals [85]. Anions such as HCO_3^- and CO_3^{2-} could react with $^{\bullet}OH$, $SO_4^{\bullet-}$, and $^{\bullet}Cl$ to yield $CO_3^{\bullet-}$ with lower oxidation potential ($E^0 = 1.57$ V *vs.* NHE) (Fig. 3b) [64]. Moreover, a stronger inhibition effect was observed at higher concentrations of cations and anions [113]. In addition, the coexisting DOM could significantly inhibit the degradation of FQs in UV/catalyst [56,60,118], UV/H_2O_2 [62,111], UV/Fenton [113], UV/PS [34,35,62,116], and UV/chlorine [34,37,38,63] processes, because of the light attenuation effect, adsorption on the surface of catalysts, and competition with the reactive species [124].

5. Assessment of the degradation pathways of FQs in UV-AOPs

Formation of TPs is concerned in UV-AOPs since they have potential hazards to ecosystem. As seen from Table S1 (Supporting information), different FQs share the same core structure of the piperazine and quinolone moiety, thus the major reactive sites and transformation routes of FQs generally exhibit a consistent pattern [125]. CIP, as the most investigated FQ in the past five years (Fig. 1b), was used as a representative for illustrating the degradation pathways of FQs in UV-AOPs. A total of 87 TPs of CIP were reported in various UV-AOPs (Table S11 in Supporting information). Among them, 12 TPs were identified in at least three types of UV-AOPs, which were used for predicting the typical degradation pathways. Density functional theory (DFT) calculation interpreted that the N atom of piperazine ring, F atom, and C2/C6 in the benzene ring were the most active sites in CIP for $^{\bullet}OH$ and $SO_4^{\bullet-}$ attack to initiate the reactions [58]. Generally, four degradation pathways of CIP were proposed including (I) hydroxylation, (II) decarboxylation, (III) defluorination, and (IV) oxidation and dealkylation of the piperazine ring (Fig. 5).

In pathway I, TP348 and TP364 with different isomers (Fig. 5 and Table S11 in Supporting information) were monohydroxyl and dihydroxyl products formed by the addition of $^{\bullet}OH$, which were commonly identified in UV/catalyst [43-45,56,58,80,82], UV/Fenton [84], UV/PS [115], UV/chlorine [126], and combined UV-AOPs [127]. In pathway II, CIP underwent decarboxylation to produce TP288a since the carboxyl group on the quinolone ring is a strong electron-withdrawing group that easily attacked by $^{\bullet}OH$. TP288a was reported in UV/catalyst [45,128], UV/Fenton [84], and UV/chlorine [57] processes.

Defluorination (pathway III) is an important pathway for FQs to reduce the toxicity, with the formation of TP330 and TP245 in various UV-AOPs (Fig. 5 and Table S11 in Supporting information). TP330 was likely generated by the substitution of the F atom on C7 by $^{\bullet}OH$, which was reported in UV/catalyst [56,58] and UV/chlorine

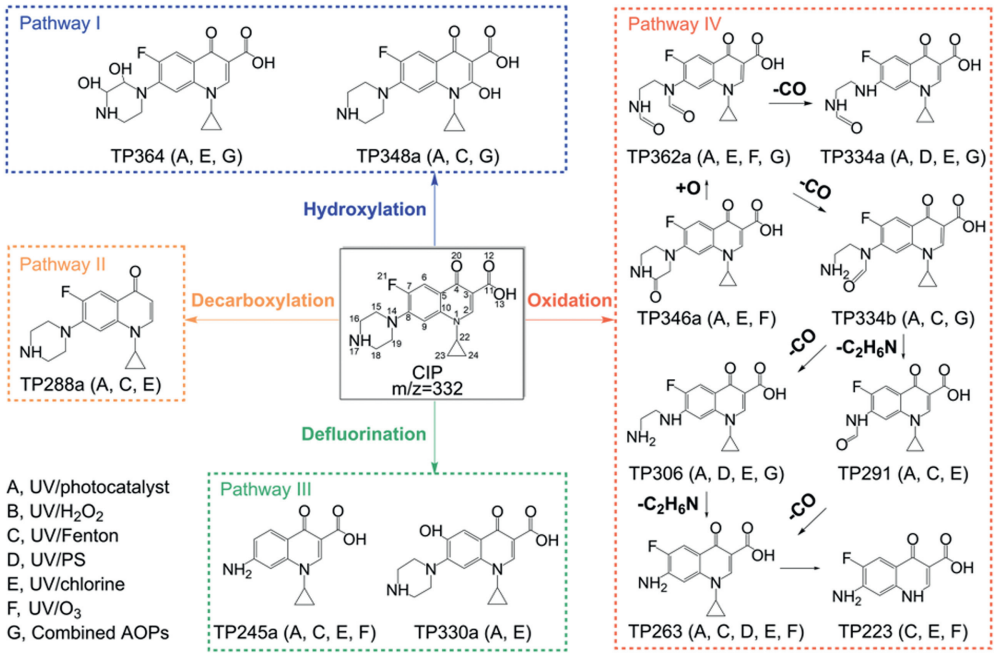

Fig. 5. Typical transformation pathways of ciprofloxacin (CIP) in different UV-AOPs.

[126] processes. TP245 were formed by defluorination and dealkylation on the piperazine ring, which were reported in UV/catalyst [44,45,58,74,128], UV/Fenton [53], UV/chlorine [126], and UV/O_3 [40] processes.

Oxidation and cleavage of the piperazine ring were proposed in pathway IV, which is easily attacked by electrophilic radicals in the FQs structure. The introduction of keto group into the piperazine ring led to the formation of TP346a, which was reported in UV/catalyst [43], UV/chlorine [126], and UV/O_3 [40]. Further oxidation and cleavage of the piperazine ring caused the generation of TP362. Consequent loss of a −CO group led to the formation of TP334a and TP334b. TP362 was reported in both UV/catalyst [44,45,58], UV/chlorine [57,126], and combined UV-AOPs [127], while TP334a and TP334b were identified in UV/catalyst [43-45,56,58,80], UV/Fenton [53], UV/PS [115], UV/chlorine [126], and combined UV-AOPs [127]. TP291 could be generated from dealkylation of TP334b, which was identified in UV/catalyst [44,45,56,58,74], UV/Fenton [53,129], and UV/chlorine [126] processes. TP306 and TP263 are partial and full dealkylation products of piperazine ring in CIP, which could also be generated from decarbonylation of TP334b and TP291. TP306 and TP263 were frequently detected in UV-AOPs including UV/catalyst [43-45,56,58,74,80,128], UV/Fenton [53,84,129,130], UV/PS [115], UV/chlorine [37,57,126], UV/O_3 [40], and combined UV-AOPs [127]. TP223 could be formed by losing a cyclopropyl group from TP263, which was reported in UV/Fenton [53], UV/chlorine [37], and UV/O_3 [40] processes.

6. Conclusions and perspectives

From the recent advances summarized in this review, UV-AOPs exhibited excellent performance in the abatement of FQs with great potential in practical application. Photocatalysis process was most extensively investigated among various UV-AOPs, with great efforts on developing metal-based, carbon-based, and metal−carbon hybrid photocatalysts. UV/PS and UV/PAA were newly developed as alternatives in FQs abatement, characterized by the formation of $SO_4^{\bullet-}$ and peroxyl radicals, respectively, in addition to $^{\bullet}OH$. The UV light intensity, dosage of catalysts/oxidants, solution pH, and water matrix components directly impacted the formation and decay of reactive species thus the degradation of FQs. Typical degradation pathways of FQs in UV-AOPs included hydroxylation, decarboxylation, defluorination, and oxidation and cleavage of piperazine ring.

However, recent advances in UV-AOPs are mostly based on bench-scale experiments and the following aspects need to be addressed for practical application. Firstly, flexible design of continuous flow UV reactors is critically important to achieve satisfactory removal efficiency of FQs both in homogeneous and heterogeneous UV-AOPs. Although the energy efficient and environment friendly UV-LEDs serve as alternatives of conventional UV lamps, future works are needed to enhance the synergistic action of UV light and oxidants/catalysts in the long-term operation. Secondly, most studies evaluated the degradation performance of UV-AOPs in synthetic wastewater by spiking individual FQs, and investigation on the removal efficiency of FQs with co-existing pollutants and water matrix components in real wastewater is still needed in future. Lastly, the toxicity of byproducts arising from antibiotic degradation should be carefully monitored in UV-AOPs for process optimization, risk assessment, and pollution control.

Declaration of competing interest

The authors declare that they have no known competing financial interests or personal relationships that could have appeared to influence the work reported in this paper.

CRediT authorship contribution statement

Huijuan Li: Writing – original draft, Visualization, Data curation. **Zhu Wang:** Visualization, Investigation, Formal analysis. **Jiagen Geng:** Visualization, Formal analysis, Data curation. **Ruiping Song:** Writing – review & editing, Supervision. **Xiaoyin Liu:** Supervision, Conceptualization. **Chaochen Fu:** Writing – review & editing, Supervision. **Si Li:** Writing – review & editing, Writing – original draft, Funding acquisition, Conceptualization.

Acknowledgments

We acknowledge the financial support from National Natural Science Foundation of China (Nos. 52100204 and

52330005) and Beijing Outstanding Young Scientist Program (No. BJJWZYJH01201910004016).

Supplementary materials

Supplementary material associated with this article can be found, in the online version, at doi:10.1016/j.cclet.2024.110138.

References

[1] S. Bhatt, S. Chatterjee, Environ. Pollut. 315 (2022) 120440.
[2] E.Y. Klein, T.P. Van Boeckel, E.M. Martinez, et al., Proc. Natl. Acad. Sci. U. S. A. 115 (2018) E3463–E3470.
[3] D. Schar, E.Y. Klein, R. Laxminarayan, et al., Sci. Rep. 10 (2020) 21878.
[4] Q.Q. Zhang, G.G. Ying, C.G. Pan, et al., Environ. Sci. Technol. 49 (2015) 6772–6782.
[5] I.T. Carvalho, L. Santos, Environ. Int. 94 (2016) 736–757.
[6] X. Van Doorslaer, J. Dewulf, H. Van Langenhove, K. Demeestere, Sci. Total Environ. 500 (2014) 250–269.
[7] M. Zou, W. Tian, J. Zhao, et al., Process Saf. Environ. Prot. 160 (2022) 116–129.
[8] S. Li, W. Shi, W. Liu, et al., Sci. Total Environ. 615 (2018) 906–917.
[9] S. Li, Y. Liu, Y. Wu, et al., Natl. Sci. Open. 1 (2022) 20220029.
[10] E.M. Golet, A.C. Alder, W. Giger, Environ. Sci. Technol. 36 (2002) 3645–3651.
[11] M. Sturini, A. Speltini, F. Maraschi, et al., Chemosphere 134 (2015) 313–318.
[12] Z. Li, J. Wang, J. Chang, et al., Sci. Total Environ. 857 (2023) 159172.
[13] R. Anjali, S. Shanthakumar, J. Environ. Manage. 246 (2019) 51–62.
[14] Y. Zhang, Y.G. Zhao, F. Maqbool, Y. Hu, J. Water Process. Eng. 45 (2022) 102496.
[15] Y. Chuang, S. Chen, C. Chinn, W. Mitch, Environ. Sci. Technol. 51 (2017) 13859–13868.
[16] C. Wang, N. Moore, K. Bircher, et al., Water Res. 161 (2019) 448–458.
[17] J. Rodriguez-Chueca, S. Varella della Giustina, J. Rocha, et al., Sci. Total Environ. 652 (2019) 1051–1061.
[18] J. Rodríguez-Chueca, E. Laski, C. García-Cañibano, et al., Sci. Total Environ. 630 (2018) 1216–1225.
[19] Y. Chen, J. Yang, L. Zeng, M. Zhu, Crit. Rev. Environ. Sci. Technol. 52 (2022) 1401–1448.
[20] S. Shurbaji, P.T. Huong, T.M. Altahtamouni, Catalysts 11 (2021) 437.
[21] Y. Gou, P. Chen, L. Yang, et al., Chemosphere 270 (2021) 129481.
[22] X. Liu, Y. Zhou, J. Zhang, et al., Chem. Eng. J. 347 (2018) 379–397.
[23] T. Song, G. Li, R. Hu, et al., Catalysts 12 (2022) 1025.
[24] Z. Lu, Y. Ling, W. Sun, et al., Environ. Pollut. 308 (2022) 119673.
[25] X. Luo, B. Zhang, Y. Lu, et al., J. Hazard. Mater. 421 (2022) 126682.
[26] H.D.M. Tran, S. Boivin, H. Kodamatani, et al., Chemosphere 286 (2022) 131682.
[27] R. Shankar, W.J. Shim, J.G. An, U.H. Yim, Water Res. 68 (2015) 304–315.
[28] W. Qiu, M. Zheng, J. Sun, et al., Sci. Total Environ. 651 (2019) 1457–1468.
[29] Y. Zhang, K. Huang, Y. Zhu, et al., RSC Adv. 12 (2022) 10088–10096.
[30] X. Zeng, Y. Meng, X. Sun, et al., J. Environ. Chem. Eng. 9 (2021) 106608.
[31] X. Ao, W. Wang, W. Sun, et al., Water Res. 203 (2021) 117458.
[32] K. Guo, Z. Wu, S. Yan, et al., Water Res. 147 (2018) 184–194.
[33] H. Milh, X. Yu, D. Cabooter, R. Dewil, Sci. Total Environ. 764 (2021) 144510.
[34] H. Yang, Y. Li, Y. Chen, et al., Water Environ. Res. 91 (2019) 1576–1588.
[35] H. Xue, S. Gao, N. Zheng, et al., Water Sci. Technol. 79 (2019) 2387–2394.
[36] C.C. Lin, H.Y. Lin, Desalin. Water Treat. 167 (2019) 170–175.
[37] J. Deng, G. Wu, S. Yuan, et al., J. Photochem. Photobiol. A: Chem. 371 (2019) 151–158.
[38] X. Zhang, K. Guo, Y. Wang, et al., Chem. Eng. J. 400 (2020) 125222.
[39] J. Lu, J. Li, J. Xu, et al., J. Water Process Eng. 44 (2021) 102324.
[40] H. Liu, Y. Gao, J. Wang, et al., Chemosphere 276 (2021) 130220.
[41] D. Krakko, A. Illes, V. Licul-Kucera, et al., Chemosphere 275 (2021) 130080.
[42] Q. Ping, T. Yan, L. Wang, et al., Water Res. 210 (2022) 118019.
[43] Q. Wu, Z. Que, Z. Li, et al., J. Hazard. Mater. 359 (2018) 414–420.
[44] C. Zhao, Y. Li, H. Chu, et al., J. Hazard. Mater. 419 (2021) 126466.
[45] K. Saravanakumar, C.M. Park, Chem. Eng. J. 423 (2021) 130076.
[46] V.T. Le, V.A. Tran, D.L. Tran, et al., Chemosphere 270 (2021) 129417.
[47] J. Lei, B. Chen, L. Zhou, et al., Chem. Eng. J. 400 (2020) 125902.
[48] J. Li, Z. Xia, D. Ma, et al., J. Colloid Interface Sci. 586 (2021) 243–256.
[49] Q. Chen, M. Zhang, J. Li, et al., Chem. Eng. J. 389 (2020) 124476.
[50] Q. Zhang, F. Han, Y. Yan, et al., Appl. Surf. Sci. 485 (2019) 547–553.
[51] R. Du, P. Chen, Q. Zhang, G. Yu, Chemosphere 273 (2021) 128435.
[52] X. Zeng, X. Sun, Y. Yu, et al., Chem. Eng. J. 378 (2019) 122226.
[53] L. Yang, Y. Xiang, F. Jia, et al., Appl. Catal. B: Environ. 292 (2021) 120198.
[54] Y. Tian, X. He, W. Chen, et al., Sci. Total Environ. 723 (2020) 138144.
[55] O. Autin, C. Romelot, L. Rust, et al., Chemosphere 92 (2013) 745–751.
[56] S. Li, J. Hu, Water Res. 132 (2018) 320–330.
[57] T.K. Kim, T. Kim, H. Park, et al., Chem. Eng. J. 394 (2020) 124803.
[58] S. Li, T. Huang, P. Du, et al., Water Res. 185 (2020) 116286.
[59] S. Guerra-Rodriguez, A.R. Lado Ribeiro, R.S. Ribeiro, et al., Sci. Total Environ. 770 (2021) 145299.
[60] P. Chen, L. Blaney, G. Cagnetta, et al., Environ. Sci. Technol. 53 (2019) 1564–1575.
[61] D. Cheng, H. Liu, E. Yang, et al., Sci. Total Environ. 773 (2021) 145102.
[62] X. Liu, Y. Liu, S. Lu, et al., Chem. Eng. J. 385 (2020) 123987.
[63] W.K. Ye, F.X. Tian, B. Xu, et al., Sep. Purif. Technol. 280 (2022) 119846.
[64] D.A. Armstrong, R.E. Huie, W.H. Koppenol, et al., Pure Appl. Chem. 87 (2015) 1139–1150.
[65] J. Lee, U. von Gunten, J.H. Kim, Environ. Sci. Technol. 54 (2020) 3064–3081.
[66] T. Luukkonen, T. Heyninck, J. Rämö, U. Lassi, Water Res. 85 (2015) 275–285.
[67] H. Zhang, L. Chen, P. Du, et al., Environ. Sci. Technol. 58 (2024) 3506–3519.
[68] M. Sturini, F. Maraschi, A. Cantalupi, et al., Materials 13 (2020) 537.
[69] M. Eskandari, N. Goudarzi, S.G. Moussavi, Water Environ. J. 32 (2018) 58–66.
[70] E.A. Serna-Galvis, Y. Avila-Torres, M. Ibanez, et al., Water 13 (2021) 2154.
[71] L. Pretali, F. Maraschi, A. Cantalupi, et al., Catalysts 10 (2020) 628.
[72] A. Kaur, A. Umar, W.A. Anderson, S.K. Kansal, J. Photochem. Photobiol. A: Chem. 360 (2018) 34–43.
[73] A. Siddique, M.B. Tahir, I. Shahid, et al., Appl. Nanosci. 12 (2022) 1613–1626.
[74] L. Wolski, K. Grzelak, M. Munko, et al., Appl. Surf. Sci. 563 (2021) 150338.
[75] N. Kaur, A. Verma, I. Thakur, S. Basu, Chemosphere 276 (2021) 130180.
[76] K. Qin, Q. Zhao, H. Yu, et al., Environ. Res. 199 (2021) 111360.
[77] T. Senasu, T. Narenuch, K. Wannakam, et al., J. Mater. Sci.: Mater. Electron. 31 (2020) 9685–9694.
[78] T. Chankhanittha, V. Somaudon, T. Photiwat, et al., J. Phys. Chem. Solids. 153 (2021) 109995.
[79] W. Liu, J. Zhou, J. Yao, Ecotoxicol. Environ. Saf. 190 (2020) 110062.
[80] X. Zheng, S. Xu, Y. Wang, et al., J. Colloid Interface Sci. 527 (2018) 202–213.
[81] S. Moles, J. Berges, M.P. Ormad, et al., Environ. Sci. Pollut. Res. 28 (2021) 24167–24179.
[82] X. Huang, S. Wu, S. Tang, et al., J. Mol. Liq. 317 (2020) 113961.
[83] C. Zhang, M. Jia, Z. Xu, et al., Chem. Eng. J. 430 (2022) 132652.
[84] Q. Wu, M.S. Siddique, Y. Guo, et al., Appl. Catal. B: Environ. 286 (2021) 119950.
[85] C. Yang, X. Wang, L. Zhang, et al., J. Taiwan Inst. Chem. Eng. 115 (2020) 117–127.
[86] L. Rizzo, Environ. Sci. Water Res. Technol. 8 (2022) 2145–2169.
[87] H. Luo, Y. Zeng, D. He, X. Pan, Chem. Eng. J. 407 (2021) 127191.
[88] Y. Jiang, J. Ran, K. Mao, et al., Ecotoxicol. Environ. Saf. 236 (2022) 113464.
[89] S.K. Mondal, A.K. Saha, A. Sinha, J. Cleaner Prod. 171 (2018) 1203–1214.
[90] H. Dan, Y. Kong, Q. Yue, et al., Chem. Eng. J. 420 (2021) 127634.
[91] W. He, Z. Li, S. Lv, et al., Chem. Eng. J. 409 (2021) 128274.
[92] W. Li, Y. Wang, J. Chen, et al., Appl. Catal. B: Environ. 302 (2022) 120882.
[93] A. Hassani, J. Scaria, F. Ghanbari, P.V. Nidheesh, Environ. Res. 217 (2023) 114789.
[94] J. Yang, M. Zhu, D.D. Dionysiou, Water Res. 189 (2021) 116627.
[95] Y. Sun, D.W. Cho, N.J.D. Graham, et al., Sci. Total Environ. 664 (2019) 312–321.
[96] E. Ngumba, A. Gachanja, T. Tuhkanen, Water Environ. J. 34 (2020) 692–703.
[97] L. Wang, J. Wei, Y. Li, et al., Chem. Eng. J. 477 (2023) 147051.
[98] T. Luukkonen, S.O. Pehkonen, Crit. Rev. Environ. Sci. Technol. 47 (2017) 1–39.
[99] X. Ao, X. Zhang, S. Li, et al., J. Hazard. Mater. 445 (2023) 130480.
[100] Z. Diao, J. Jin, M. Zou, et al., Sep. Purif. Technol. 278 (2021) 119620.
[101] Z.H. Diao, S.T. Huang, X. Chen, et al., J. Cleaner Prod. 330 (2022) 129806.
[102] J. Wu, J. Bai, Z. Wang, et al., Environ. Technol. 43 (2022) 95–106.
[103] H. Tang, Z. Dai, X. Xie, et al., Chem. Eng. J. 356 (2019) 472–482.
[104] Y.h. Tian, N. Jia, L. Zhou, et al., Chemosphere 288 (2022) 132627.
[105] D. Li, Z. Feng, B. Zhou, et al., Sci. Total Environ. 844 (2022) 157162.
[106] P. Wang, H. Zhang, Z. Wu, et al., Chin. Chem. Lett. 34 (2023) 108722.
[107] F. Wang, Y. Feng, P. Chen, et al., Appl. Catal. B: Environ. 227 (2018) 114–122.
[108] G. Wang, Y. Li, J. Dai, N. Deng, Environ. Sci. Pollut. Res. 29 (2022) 48522–48538.
[109] H. Abdelraouf, J. Ding, J. Ren, et al., Process Saf. Environ. Prot. 168 (2022) 892–906.
[110] M. Kumaresan, V. Saravanan, M. Swaminathan, Inorg. Chem. Commun. 142 (2022) 109706.
[111] K. Jutarvutikul, C. Sakulthaew, C. Chokejaroenrat, et al., Aquacult. Eng. 94 (2021) 102174.
[112] A.S. Giri, A.K. Golder, J. Environ. Sci. 80 (2019) 82–92.
[113] C. Wang, J. Zhang, J. Du, et al., J. Hazard. Mater. 416 (2021) 125893.
[114] G. Harini, M.K. Okla, I.A. Alaraidh, et al., Chemosphere 303 (2022) 134963.
[115] X. Ao, W. Liu, W. Sun, et al., Chem. Eng. J. 345 (2018) 87–97.
[116] Y. Qi, R. Qu, J. Liu, et al., Chemosphere 237 (2019) 124484.
[117] S.P. Asu, N.K. Sompalli, S. Kuppusamy, et al., Mater. Today Sustain. 19 (2022) 100189.
[118] N. Yin, H. Chen, X. Yuan, et al., J. Hazard. Mater. 436 (2022) 129317.
[119] H. Guo, N. Gao, Y. Yang, Y. Zhang, Chem. Eng. J. 292 (2016) 82–91.
[120] M. Kamagate, A.A. Assadi, T. Kone, et al., J. Hazard. Mater. 346 (2018) 159–166.
[121] Y. Park, S. Kim, J. Kim, et al., Water 14 (2022) 958.
[122] F.H. Borba, A. Schmitz, L. Pellenz, et al., J. Environ. Chem. Eng. 6 (2018) 6979–6988.
[123] Y. Zhu, M. Wei, Z. Pan, et al., Sci. Total Environ. 705 (2020) 135960.
[124] S. Li, J.Y. Hu, J. Hazard. Mater. 318 (2016) 134–144.
[125] F. Tan, D. Sun, J. Gao, et al., J. Hazard. Mater. 244 (2013) 750–757.
[126] Z. Li, X. Yuan, H. Tang, et al., Environ. Sci. Water Res. Technol. 8 (2022) 2744–2760.
[127] A. Wang, H. Wang, H. Deng, et al., Appl. Catal. B: Environ. 248 (2019) 298–308.
[128] Y. Yu, K. Liu, Y. Zhang, et al., Int. J. Environ. Res. Public Health 19 (2022) 4793.
[129] F. Wang, X. Yu, M. Ge, S. Wu, Chem. Eng. J. 384 (2020) 123381.
[130] O. Gomes Junior, V.M. Silva, A.E.H. Machado, et al., J. Environ. Manage. 213 (2018) 20–26.